Original Paper

Control of Pump Performance with Attaching Flaps on Blade Trailing Edges

Yuji Kanemori[1] and Ying Kang Pan[1]

[1] Research and development Department, Torishima Pump MFG. co., Ltd.
1-1-8, Miyata-cho Takatsuki-shi, Osaka, Japan

Abstract

An innovative method of changing a centrifugal low specific speed pump performance and pressure fluctuation by applying outlet flaps to impeller exit has been investigated. The outlet blade edge section corresponds to the trailing edge of wing on the circular-cascade, which dominates the pump performance and pressure fluctuation. Computational fluid dynamics (CFD) analysis of the entire impeller and volute casing and an experimental investigation are conducted. The pressure fluctuation and the vibration of the shaft are measured simultaneously. Kurtosis is applied as a dimensionless parameter with which the unevenness of velocity distribution at impeller outlet is indicated. The influence of the flaps on the pressure fluctuation is explained by the kurtosis. This paper presents a theoretical method of predicting the pump performance related to the attachment of a flap at impeller outlet.

Keywords: Pump, Flap, Performance, Pressure fluctuation, Vibration

1. Introduction

A pump is usually designed according to a specification associated with the maximum impeller diameter. Therefore, when higher head or discharge is demanded, a larger impeller diameter is required. In order to make a slight improvement in head-capacity curve, without changing the impeller diameter, under-filing could be used. Thus, modifying suction side surface shape of impeller outlets is a method to achieve a modest gain in head, to change the area and the angle of the impeller outlet. Another method to modify pump performance is to attach flaps on impeller blade outlets. Impeller and guide vanes of the turbo machine such as pump and water turbine and blower are part of star cascade where the wings are arranged circularly at regular intervals. The blade trailing edge shape is a part that greatly influences the performance of the turbo machine [1]. Thinly processing suction side of the wing will permit to operate a sensitive part of this cascade.

Inversely to the under-filing of blade outlets, an innovative method to control pump performance is the formation of flaps at impeller blade outlets [2]. The impeller outlet corresponds to blade trailing edge of the wing cascade, and the blade trailing edge shape of the wing acts greatly on the pump performance. Therefore the influence of flap at the impeller outlet on the pump performance was investigated. It is confirmed that the flap can suppress the pressure fluctuation in a two-stage low specific speed pump.

Many computational fluid dynamical analyses of flow field in pumps have been carried out and the results confirmed details that have been observed experimentally [3]. Consequently computational analysis was performed about the entire pump flow field including crossing over passages in this survey.
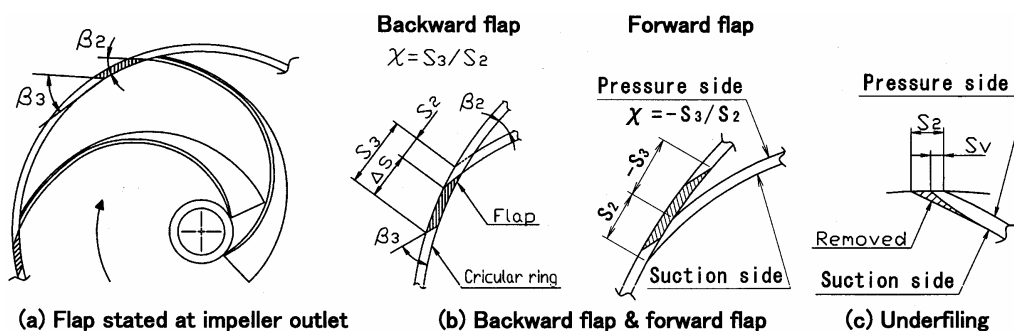

Fig. 1 Impeller trailing edge shapes

(a) Flap stated at impeller outlet   (b) Backward flap & forward flap   (c) Underfiling

A numerical study of unsteady flow in a centrifugal pump was conducted and it has been demonstrated that the interaction between impeller and volute casing flow is characterized with pressure fluctuations, which are strong at the impeller outlet and the vicinity of the tongue [4]. By the way, kurtosis is employed by diagnosis of the vibration [5] as the parameter with which breakdown is judged. Referring to the diagnosis, the kurtosis was introduced as a parameter which indicates suction influence of the pressure fluctuation to evaluate the unevenness of impeller discharge flow field.

Research of the low specific speed pump has progressed technology and a great amount of data has been accumulated [6]. However the performance adjustment has not yet been achieved with the centrifugal pump, although it has been realized with the movable vanes of the axial and mixed flow pumps.

The aim of this paper is to establish a technique of the performance adjustment with the attachments on the blade trailing edge concerning a centrifugal pump. The performance change of the low specific speed pump with the attachment on blade was theoretically analyzed by using the slip factor after Wiesner [7]. To evaluate experimentally the change in the pressure fluctuation with the circular-cascade wing ring, the pump rotational speed has been varied quasi-statically [8]. The rotational speed at which the pressure fluctuation reaches the maximum was defined at this time, and the influence of the blade trailing edge shape on the pressure fluctuation was studied theoretically and experimentally. The pressure fluctuation without flap wings was compared with other documents [9] [10]. The interrelation of the shape of the outlet trailing edge and the pressure fluctuation was studied [11]~[14]. In order to alter the pressure fluctuation intentionally, the flap position of the blade edge at impeller outlet was changed. Moreover, the magnitude of the pressure fluctuation is explained by the kurtosis. The effectiveness of the attaching flap on the blade trailing edge was presented from the relationship between this pressure fluctuation and shaft vibration.

2.   The test pump and numerical model

2.1 Pump characteristic and computational modeling

Figure 2 shows a schematic of the two-stage turbine pump used for this experiment. Two impellers are placed in back to back type position in order to counterbalance the axial thrust. Crossing-over flow pass was adopted as a connecting passage where the discharged water of first stage impeller is led to next suction bay.   Design-specific speed of impeller for single stage is Ns=100 (min^{-1}, m^3/min, m), where the dimensionless type number n_s^* is 0.244. Hence the specific speed of the two stage of the pump machine is 60 (Ns=100/2$^{3/4}$≒60). The pump was investigated theoretically and experimentally.
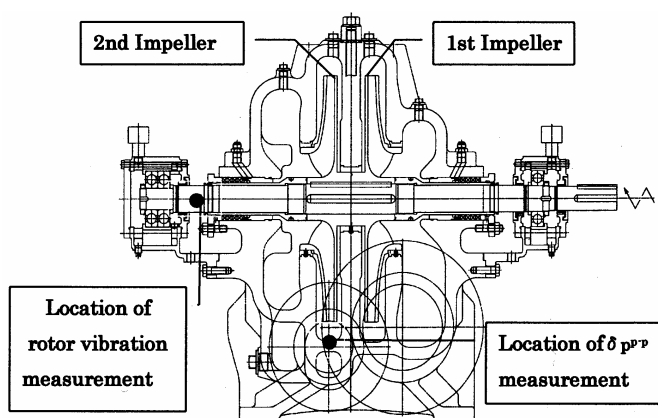

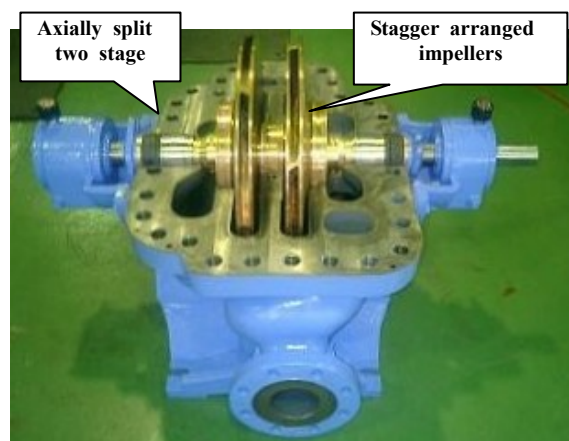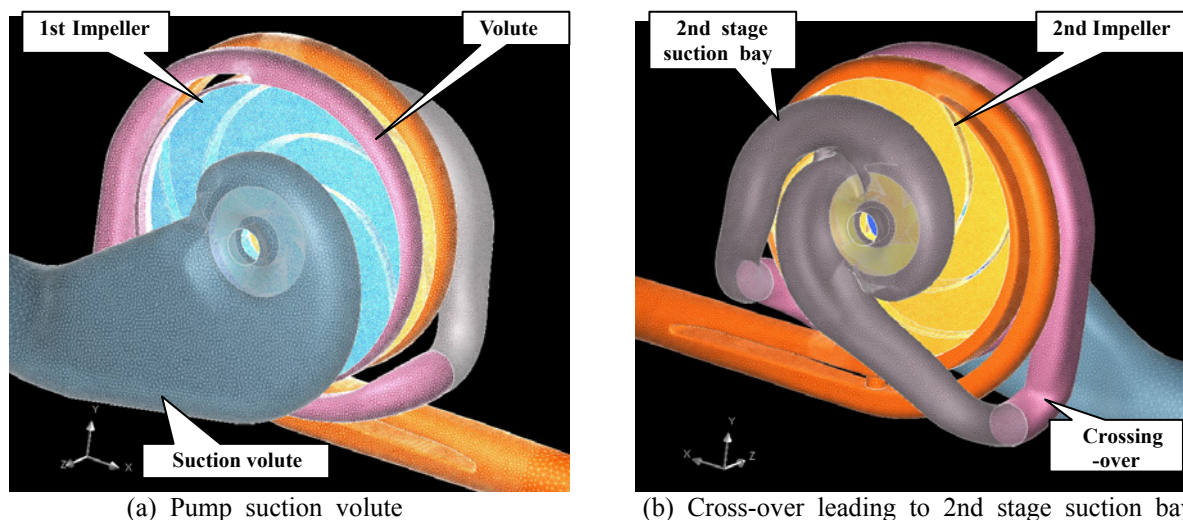**Fig. 2** The test pump showing location of pressure tap

Fig. 3 Photograph of Impellers in the test section

(a) Pump suction volute

(b) Cross-over leading to 2nd stage suction bay

Fig. 4 Numerical model

The entire pump flow field including crossing-over passages was analyzed by CFD (Computational Fluid Dynamics). Figure 4 shows supplied computing model grid for the test pump as mentioned in Fig. 2. In this paper, a general purpose comercial code (Scryu/Tetra) with non-structural mesh to solve Reynolds averaged incompressible Navier-Stokes equations was employed. The function of a discontinuous joint was used to connect an analytical area between the rotating impeller and geostationary suction and discharge volute by using standard k-ε turbulence model. The boundary condition is defined by assuming that the pressure is constant at the entrance suction pipe and similarly the flow quantity at the discharge pipe outlet is constant.

The passage shape was decided so that the kinetic energy of two crossing-overs connected from double volutes is efficiently converted into pressure energy. Moreover, an appropriate pre-swirl to the inlet flow of the impeller suction casing is designed to normalize the pressure distribution in the suction casing. Table 1 shows the pump specification used for the experiment and numerical analysis.

The tongue skew ratio of supplied pump is zero and the tongue distance ratio ξ between double volute tongue and impeller outlet gap is $\xi = \{a + (D_c - D_3)/2\}/D_3 = 0.055$.

Table 1 Pump characteristic data

Impeller width	b_2	19(mm)	Blade thickness	t	8(mm)
Impeller eye diameter	D_1	211(mm)	Blade number	Z	6
Flap ring diameter	D_3	530(mm)	Impeller outlet angle	β_2	25(deg)
Base circle diameter	D_c	580(mm)	Flap exit angle	β_3	0 and 25(deg)
Design specific speed	Ns	100	Tetrahedra Grid-Number	—	2.45E+06

2.2 Shape of blade trailing edge flap installed at impeller discharge

In this research, two kinds of blade trailing edge flap rings, shown in Fig.5, were installed at impeller discharge of the first and second stages. The pump performance and pressure fluctuation with the same ring diameter in which blade trailing edge flap exit angle β_3 of 0 degree and 25 degrees were carried out. The position of circular-cascade wing ring is changeable and the installation position of the blade trailing edge flap ring can be changed as shown in Fig.5.

Fig. 5 Circular-cascade wing ring shapes used in experiment

The installation positions of blade trailing edge flaps are as follows.

(a) Usual state of $\chi=1$ by which blade trailing edge flap becomes a part of vane of impeller (Normal). Under such a condition, the flap becomes an element of vane as well as a usual impeller blade.

(b) State of $\chi<0$ (Forward)

The flap located on forward position. The flap is set so as to protrude from the pressure side of the blade in the rotational direction. Concerning the state of the extension of blade trailing edge flap in the rotational direction, that is $\chi=-1$ or -2, the minus sign $\chi= (-)$ is defined as forward.

(c) State of $\chi>1$ (Backward)

The trailing edge of circular-cascade wing ring retreats to the suction side of impeller. The state of the opposite extension of blade trailing edge flap with the reverse rotational direction, namely, $\chi=2$ and $\chi=3$ is defined as backward.

(d) Separated cascade wing ring being installed far from the edge of the suction side of impeller vane, which changes lift of impeller vane by circular-cascade wing ring flap, as shown in Fig.5 (d). The distance between the leading edge of flap and the trailing edge of blade is the same as the impeller outlet vane tips length S_2.

The setting position of the first stage and the second stage impellers is mutually fixed as a half pitch phase from each other, eventually staggered arrangement as shown in Fig.3.
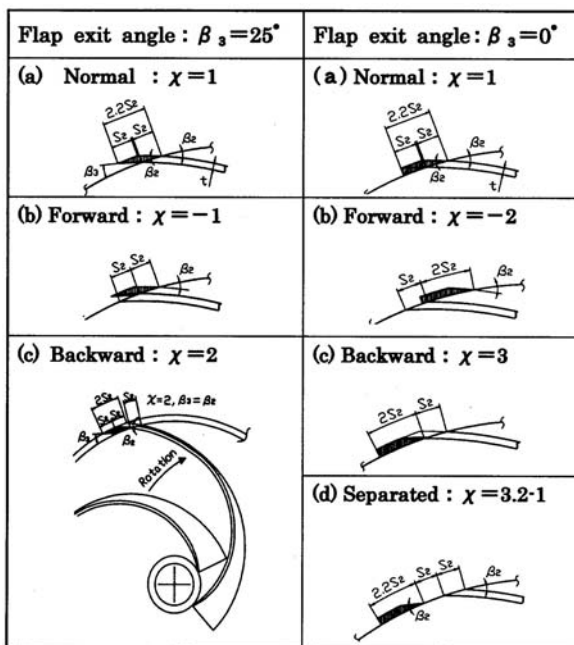
3. Numerical prediction of the pump performance

Computational analysis was performed by the numerical model shown in Fig.4 at the pump best efficiency of flow rate. Figure 6 shows the flow velocity vectors in the first stage impeller mid-span and the center passage part of double volute. Figure 7 shows the velocity vectors in the suction port of the second stage and discharge volute.

The mass flow rate through the two crossing-over passages becomes almost equivalent. Flow separation and vortex did not occur from the velocity distribution of the second stage suction bay, as shown in Fig.7, and it was confirmed that the flow of the suction is uniform without flow disturbance.
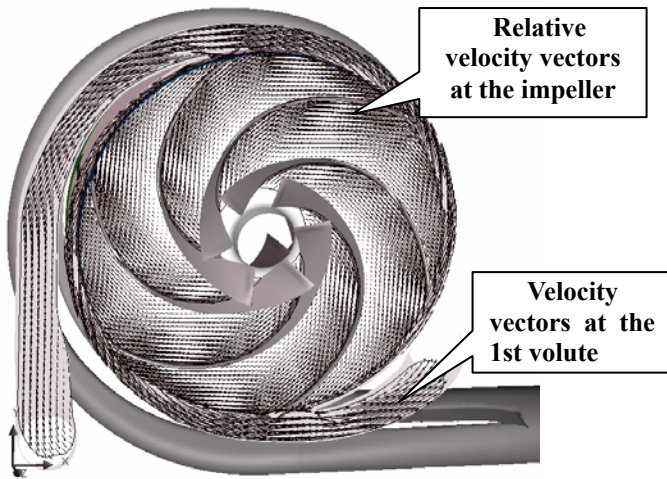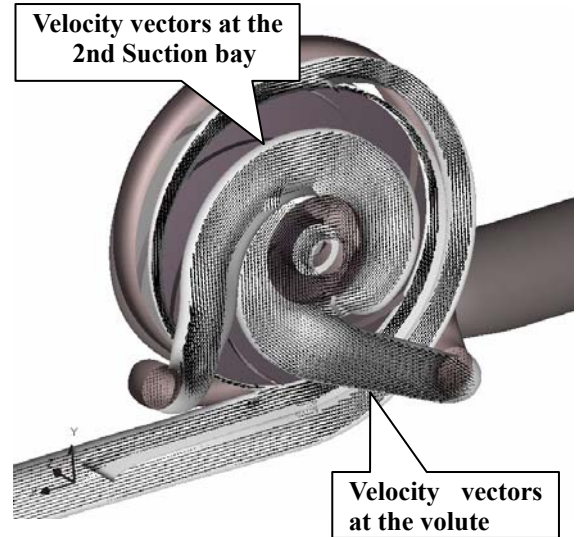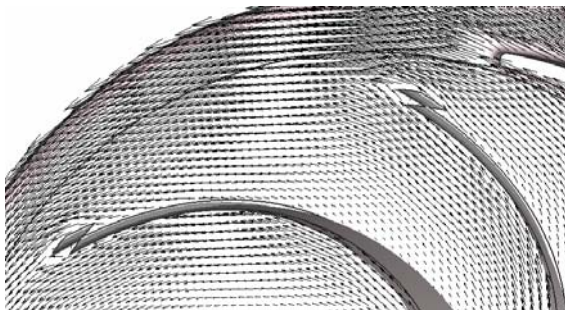
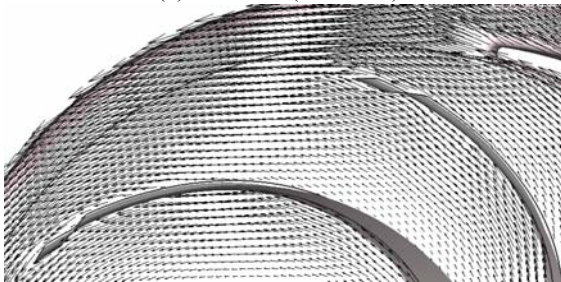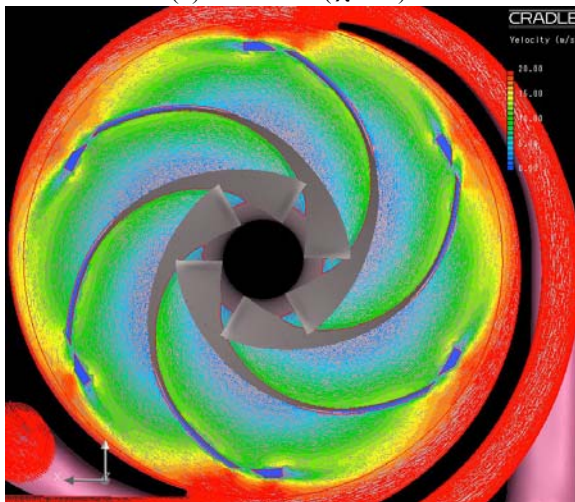**Fig. 6** Flow velocity vectors at the first impeller

Fig. 7 Velocity vectors at the 2nd Suction volute

(a) Forward ($\chi = -1$)

(b) Backward ($\chi = 2$)

(c) Separated ($\chi = 3.2$-1)

Fig. 8 Relative velocity vectors of the impeller at BEP

The influence of attachments on blade trailing edge at impeller outlet is numerically analyzed by displaying the results of flow field.

Figure 8(a) shows relative velocity vectors at impeller outlet with forward flap, in which the blade trailing edge flap ring progressed in the rotational direction. Moreover, Fig.8(b) shows the relative velocity vectors at impeller outlet in the mid-span plane by CFD in the state of backward, in which the flap is installed in the opposite direction to the rotation. The flow field of separated cascade wing ring is displayed in Fig.8(c).

In the case of backward, the stream near the blade trailing edge flap flows comes out from impeller without any significant separation on the pressure side. As the blade loading around vicinity of the impeller outlet becomes small, it is suggested that pump head changes without deteriorating efficiency.

On the other hand, in forward configuration the flow is partially stagnated near outlet on the pressure side, which increases the flow angle β_{2f} at impeller outlet. It does not seem that the flows from both the pressure and suction sides joint smoothly.

Figure 9 shows the analytical results by CFD on the blade-to-blade velocity distribution at impeller outlet.

The absolute circumferential velocity component C_{u2} and meridional velocity C_{m2} are normalized by the peripheral velocity at the impeller outlet tip, U_2. It has a physical meaning that C_{u2}/U_2 expresses the head coefficient and C_{m2}/U_2 corresponds to the flow coefficient.

The circumferential pressure distribution of the casing remains approximately constant under the pump best efficiency point.

The relative flow velocity angle at impeller outlet β_{2f} is obtained from eq. (1) as the mean value by each vane pitch.

$$\beta_{2f} = \tan^{-1} \frac{C_{m2}}{W_{u2}} \qquad (1)$$

It is obvious that the position and the shape of blade trailing edge flap at the impeller outlet influence the flow velocity distribution. The flow discharge angle β_{2f} of the vicinity of the impeller outlet increases in forward configuration. When exit angle β_3 of blade trailing edge flap is zero, both the circumferential velocity and the pump head get smaller, compared with the angle β_3 of 25 degrees.
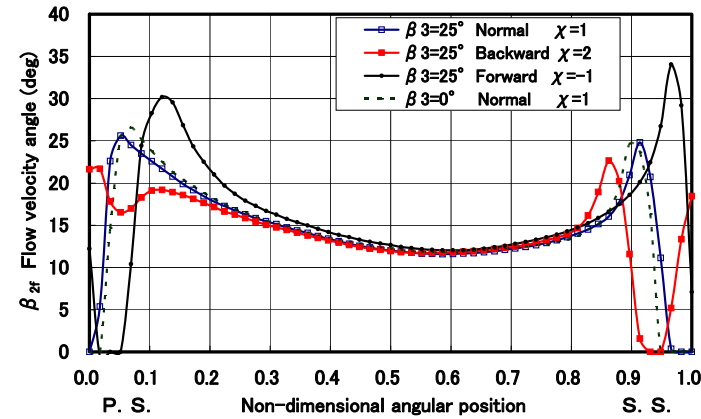
4. Kurtosis of the velocity distribution at impeller outlet

As a parameter showing the non-uniformity of the meridional velocity distribution of the impeller outlet derived from CFD, the kurtosis κ of velocity distribution (C_{m2}/U_2) between two blades was calculated. Kurtosis is usually applied to the failure diagnosis by vibrations [5]. In this paper the kurtosis κ is applied as a dimensionless parameter which the magnitude of the salient of velocity distribution at impeller outlet is indicated. Kurtosis of the velocity distribution at impeller outlet (C_{m2}/U_2) is obtained by Expression (2), when $\phi_i = C_{m2i}/U_2$ for flow coefficient of CFD analysis grid node
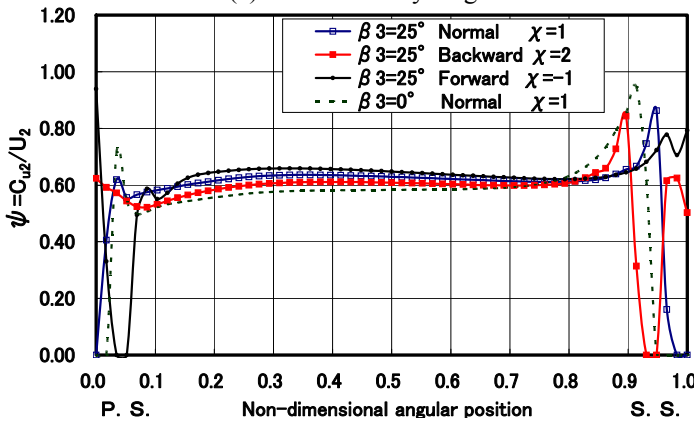
$$\kappa = \left\{ \frac{n(n+1)}{(n-1)(n-2)(n-3)} \Sigma \left(\frac{\phi_i - \phi_{ave}}{\phi_s} \right)^4 \right\} - 3 \frac{(n-1)^2}{(n-2)(n-3)} \tag{2}$$

where ϕ_S shows the standard deviation of ϕ_i, ϕ_{ave} shows the mean value of ϕ and n is the total node number.
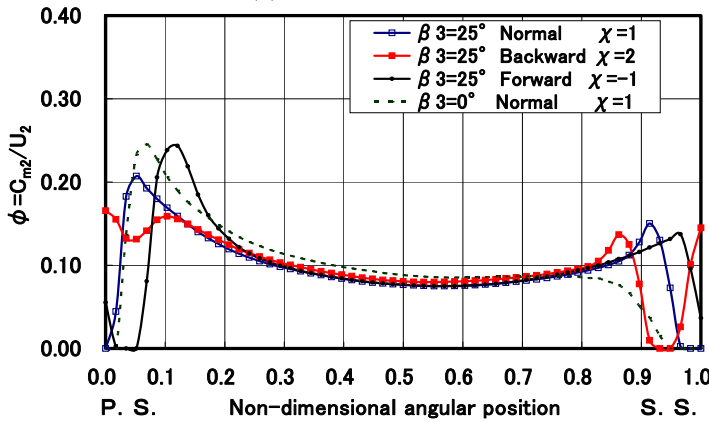
Figure 10 displays the analytical results of mean flow velocity angle β_{2f} and the kurtosis κ at impeller discharge by CFD.

The kurtosis κ means a level of distortion in the velocity distribution because κ increases when the level of salient velocity distribution at impeller discharge sharpens.

In the forward configuration ($\chi<0$), the mean flow velocity angle β_{2f} enlarges and kurtosis κ also increases.

On the other hand, the more β_{2f} gets smaller for backward configuration ($\chi>1$), the more the kurtosis decreases.

Therefore, the kurtosis κ indicates the level of the circumferential unevenness of impeller discharge flow. The pressure fluctuation and pump performance will be altered because both the impeller discharge area and the flow velocity angle β_{2f} are changed by moving blade trailing edge flap.

Rotor-stator interaction should be divided into two mechanisms. The first is potential flow interaction and the second is wake interaction. Since the radial gap between the tongue and impeller outlet is small, potential flow interaction may be predominant.
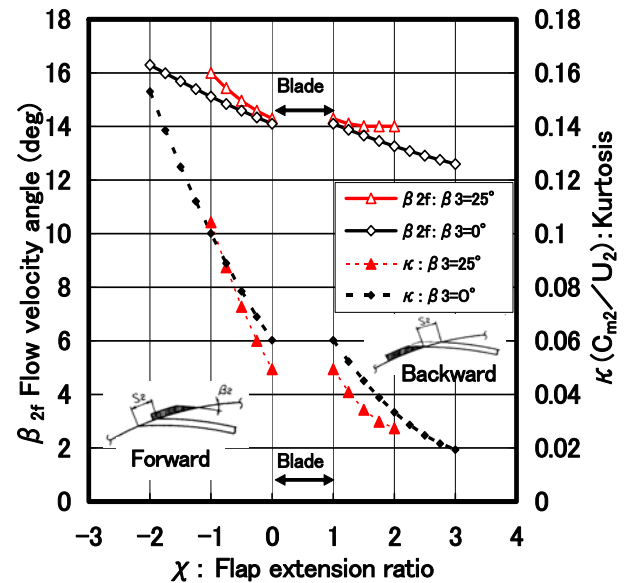

(a) Flow velocity angle

(b) Head coefficient

(c) Flow coefficient

Fig. 9 Blade-to-blade velocity distributions at impeller outlet

Fig. 10 Effect of flap on flow velocity angle and Kurtosis by CFD ($Q/Q_d=1$)

5. Prediction of pump characteristics with flap attachment

An impeller outlet blade vector $\vec{F}^{*}_{2}$ is expressed to be an averaged vector of the impeller pressure side blade vector $\vec{F}_{2}$ and suction side blade vector $\vec{F}_{2S}$ by installing a flap at the blade trailing edge from the relative velocity vectors shown in Fig.11.

$$\vec{F}^{*}_{2}=(\vec{F}_{2}+v\vec{F}_{2S})/2 \tag{3}$$

The exit blade angle of the suction side β_{2S} corresponding to blade trailing edge flap may be derived from the relationship between the tip width S_3 and flap thickness "e". The blade angle of suction side β_{2S} with attaching flap ΔS is given by

$$\beta_{2S}=\sin^{-1}\{e / (\Delta S+S_2)\} \tag{4}$$

When the flap length ΔS is zero, β_{2S} becomes $\sin^{-1}(e / S_2)$ which is consistent with the normal blade.

The ratio v obtained by angular difference between the blade trailing edge flap β_3 and the impeller blade angle β_2 is stated

$$v=\sin(\beta_2-\beta_3) \tag{5}$$

If β^{*}_{2} is supposed to be an angle of the vector $\vec{F}^{*}_{2}$ which is illustrated in Fig.11.

$$\beta^{*}_{2}=\tan^{-1}\left\{\left(\sin\beta_2+v\sin\beta_{2S}\right)\middle/\left(\cos\beta_2+v\cos\beta_{2S}\right)\right\} \tag{6}$$

When β_3 and β_2 are the same, eq. (6) becomes $\beta^{*}_{2}=\beta_2$

Impeller blade angle β_2 will be changed to β^{*}_{2} as explained by eq. (6) with attaching the blade trailing edge flap.

The effect of the blade trailing edge flap on head and flow rate at the best efficiency is predicted by eqs. (7) and (8) concerning β^{*}_{2}, respectively [6].

$$H_{BFP}=\frac{U_2^{2}}{g}\frac{(1-k_2)}{\left\{1+B_c\ln\left(1+\frac{2B_c}{D_c}\right)\middle/\left(2\pi\varepsilon_2 b_2\tan\beta^{*}_{2}\right)\right\}} \tag{7}$$
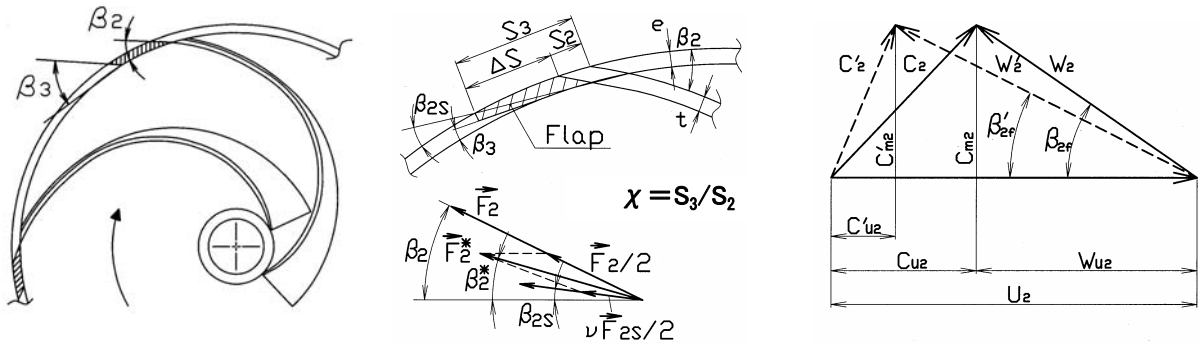
$$Q_{BEP}=\frac{(\pi\varepsilon_2 b_2 D_2)U_2(1-k_2)}{2\pi\varepsilon_2 b_2/B_c\ln\left(1+\frac{2B_c}{D_c}\right)+1/\tan\beta^{*}_{2}} \tag{8}$$

Here ε_2 is the reduction ratio of impeller discharge area and Wiesner's slip factor k_2 is as follows [7]

$$\varepsilon_2=(\pi D_2-ZS_3)/\pi D_2 \tag{9}$$

$$k_2=\sqrt{\sin\beta^{*}_{2}}/Z^{0.7} \tag{10}$$

The relative flow velocity angle at impeller outlet β_{2f} is changed to β'_{2f} by installing a flap, and the circumferential absolute velocity change provides significant influence on pump performance.

(a) Impeller outlet blade vectors with attaching flap (b) Discharge flow velocity triangles
Fig. 11 Circular ring flap stated at impeller outlet

6. Experimental apparatus and procedure

The experiment was conducted in accordance with JIS B 8301 code Grade 1 by using the normal temperature water with an electromagnetic flow meter, a torque measuring instrument, a tachometer, and a pressure transducer. When the pump performance test was carried out, the pressure fluctuation and the shaft vibration were measured simultaneously. The strain-gauge type pressure transducer was used to measure the pressure fluctuation. The natural frequency of the transducer attains 23kHz with which the response performance is evaluated and it is higher than the NZ vane passing frequency. The calibration of the gap sensor had been conducted before measuring the pump shaft vibration. The frequency range to be able to measure the gap sensor is 10kHz. The test pump was driven by a motor with an inverter to operate at variable rotational speeds. The experiment was carried out by recirculating water in a closed-loop with a pressure tank. The suction pressure of the pump has been adjusted by changing pressure in the tank with a compressor and a vacuum pump.

6.1 Test pump performance

Figure 12 shows the test results of the pump performance curves and the numerically calculated pump efficiency by CFD. The outside of impeller has been trimmed to several diameters. The diameters of the first stage and the second stage impellers are the same. The efficiency at the best efficiency point derived from the numerical analysis at steady state condition is consistent with the actual measuring result. Specific speed increases by trimming the impeller outside diameter from $D_2=\phi 575$ to $\phi 510$. The actual measurement value of efficiency is higher than 80% within the range of specific speed from 104 to 132. ($Ns=NQ^{1/2}/h^{3/4}$: h= H /2:min^{-1},m^3/min, m), which is the dimensionless type number n_s^* changes from 0.254 to 0.327.

The CFD results show a reasonable agreement with the measured ones, thought the efficiency by CFD results tend to be underestimated compared with the measured values. It is considered that efficiency increases because the disc friction loss decreases and specific speed increases by the impeller outside diameter trimming in the range of this experiment. After confirming the accuracy of numerical model and boundary conditions, the theoretical and experimental studies were carried out.

The blade trailing edge flap ring of 10mm in thickness and $\phi 530$mm in the outside diameter of cascade wing ring was installed on the impeller outer part of $\phi 510$. The cascade wing ring was movable in the circumference direction in this experiment as shown in Fig.5. Only the position of the cascade wing ring has been changed in the pump performance test. Other parts of the impeller and the casing have remained the same in all tests.

The pump performance curve can be changed with attaching the flap as shown in Fig.12. The pump head would be controlled between the impeller diameter from $\phi 510$ to $\phi 540$mm with the blade trailing edge flap shown in fig.5 ($\beta_3=0$). As well as changing the impeller diameter, the pump performance would be controlled by changing the flap location.

6.2 Measurement of pressure fluctuation

The maximum pressure fluctuation in the pump casing is adapted as represent pressure fluctuation in the experiment. The pump rotational speed was changed in the range of $600\sim1200$(min^{-1}) to find the speed at which the pressure fluctuation in the pump casing grows to the largest. Critical rotational accelerating speed f_{cr}, where dynamic performance of the pump begins to separate from the quasi-steady state, is derived from the following empirical formula [8].

$$f_{cr}= 0.1(Z\phi/cos\beta_2)N_r \tag{11}$$

Here, the flow coefficient ϕ is 0.07 and the range of the rotational speed Nr varies from 10 to 20Hz in the experiment.

Therefore, the maximum critical rotational changing speed f_{cr} becomes 0.695Hz, and if the increment of rotational speed is less than $N_{cr}=41.71$(min^{-1}) per minute, it is possible to treat as quasi-stationary. The rotational speed increases from 600 to 1200(min^{-1}) in 14 minutes, namely accelerated 600(min^{-1}) in 14 minutes, and decelerated from 1200 to 600 (min^{-1}) in this experiment based on eq. (11). Figure 13 shows the pressure fluctuation in the casing when the pump is driven by changing the rotational speed.

In the experiment the rotational speed of the pump of 1100(min^{-1}) was selected where the pressure fluctuation reaches its maximum.

In a pump, the component of vane passing frequency NZ becomes dominant. In the experiment, the rotational speed component of the impeller, N was observed continuously. Since the NZ becomes predominant, N is smaller than the vane passing NZ.

Therefore, the rotational speed was fixed, flow rate was changed by the valve adjustment, and the pressure fluctuation at the discharge near the tongue in the casing shown in Fig.2 was measured in this experiment.

Deaeration had been done enough before the start of the experiment on pressure fluctuation. The suction pressure was kept over 0.17MPa, and noted that bubbles should not be generated while measuring.
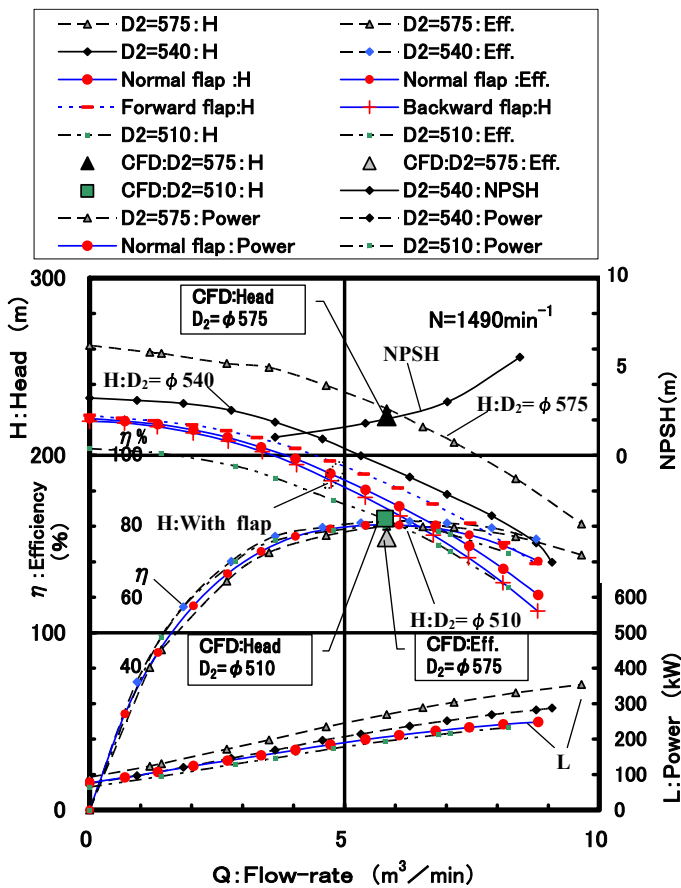

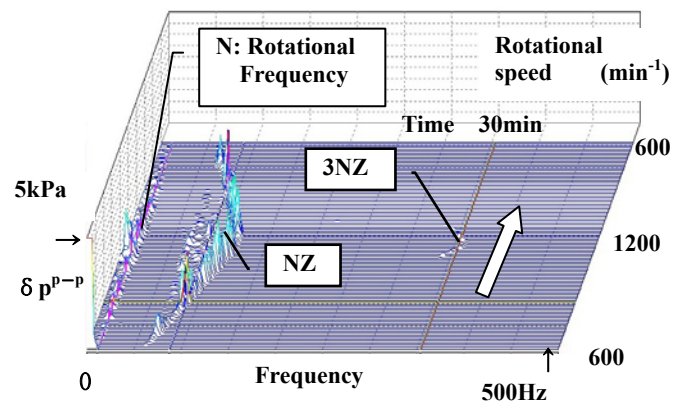**Fig. 12** Performance curves of the test pump

Fig. 13 Pressure transient behavior($D_2=\phi 530$)

7. Results of static and dynamic pump characteristics by attaching flap

7.1 Angle of exit flap on impeller blade trailing edge β_3 is 25 degrees

Figure 14 shows the position of flap ring and the relationship to the pump performance. The exit flap angle β_3 was processed to 25 degrees. For forward configuration ($\chi=-1$), efficiency decreases by (0.7%) although the pump head increases.

Oppositely for backward configuration ($\chi=2$), the pump shaft power and head decrease. However, the change in efficiency becomes (0.2%) lower. On the other hand, cavitations coefficient σ showing suction performance is not influenced by the installed position of the blade trailing edge flap ring, and σ remains equivalent.

If the exit flap angle β_3 is the same as impeller blade angle at outlet β_2 with 25 degrees, flow rate is controlled only as for the ratio of impeller discharge area reduction ratio ε_2 of eqs. (7) (8) and the effect of blade trailing edge flap is small. In the case of ($\chi=-1$), i.e. forward, the efficiency decrement is little though the head coefficient ψ increases in the pump performance, which is an interesting point.

Pump pressure fluctuation coefficient $\delta P^{p\text{-}p}$ is defined [9] as

$$\delta P^{p\text{-}p} = \delta p^{p\text{-}p}/(\gamma U_2^2/g) \qquad (12)$$

The pump pressure fluctuation is normalized using definite value $\gamma U_2^2/g$ for the sake of clarifying the relative effect of blade trailing edge flap on the pressure fluctuation instead of the alternating pump head.

Figure 14 shows the relationship between the pressure fluctuation coefficient $\delta P^{p\text{-}p}$ and the flow coefficient ϕ. Though $\delta P^{p\text{-}p}$ decreases to the minimum at BEP flow rate, $\delta P^{p\text{-}p}$ increases to its maximum during shut off and it becomes the largest at the over flow rate in any case, whatever position the blade trailing edge flap ring is set up in.

When $\chi=1$ at which blade trailing edge flap does not affect the flow discharge angle at the impeller outlet, the pump pressure fluctuation coefficient is in the range of $0.03\sim0.05$, and the magnitude is similar to the usual impeller [10]. In the case of backward configuration ($\chi=2$) in which S_2 retreats to the rear side contrary to the rotational direction, the pump pressure fluctuation $\delta P^{p\text{-}p}$ decreases as well as the pump shaft power and head.

Reversely with the forward configuration ($\chi=-1$) where S_2 progresses in the rotational direction, the pump pressure fluctuation $\delta P^{p\text{-}p}$ increases with head. That is, the ring leading edge extends in the pressure side of impeller blade and S_2 progresses in the rotational direction.

The reason why $\delta P^{p\text{-}p}$ increases on forward can be explained by the fact that flow velocity angle at impeller outlet β_{2f} of the pressure side enlarges more than 25 degrees of impeller blade angle β_2.
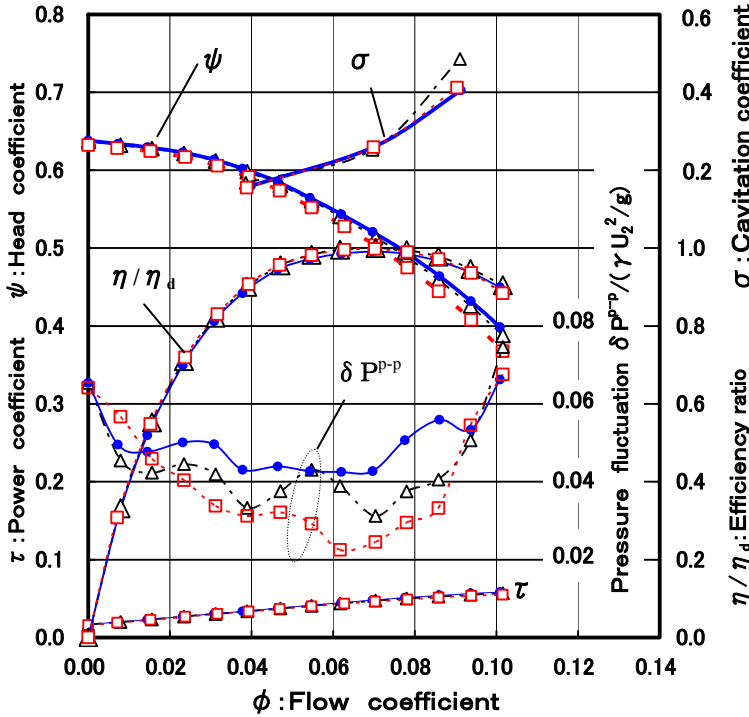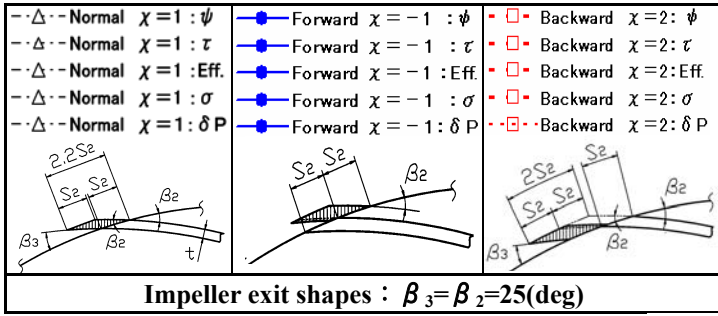

Fig.14 Pump performance curve and $\delta P^{p\text{-}p}$
(Flap exit angle: $\beta_3 = \beta_2 = 25°$)

7.2 Angle of exit flap on impeller blade trailing edge β_3 is zero degree

When the angle of exit flap on impeller blade trailing edge β_3 is 0 degree, pump performance and pressure fluctuation coefficient $\delta P^{p\text{-}p}$ are displayed in Fig.15 similar to Fig.14. Because the impeller blade angle with flap attachment β_2^* expressed by eq.(6) gets smaller, the influence of blade trailing edge flap is significant. In backward configuration ($\chi>1$), the impeller blade angle with flap β_2^* gets smaller by the effect of blade trailing edge flap. Therefore, the head coefficient ψ is low and the pressure fluctuation also decreases. As for contribution of the exit flap angle β_3 to the shaft power and head, when the exit flap angle β_3 is 0 degree, β_3 affects more than that of 25 degrees.
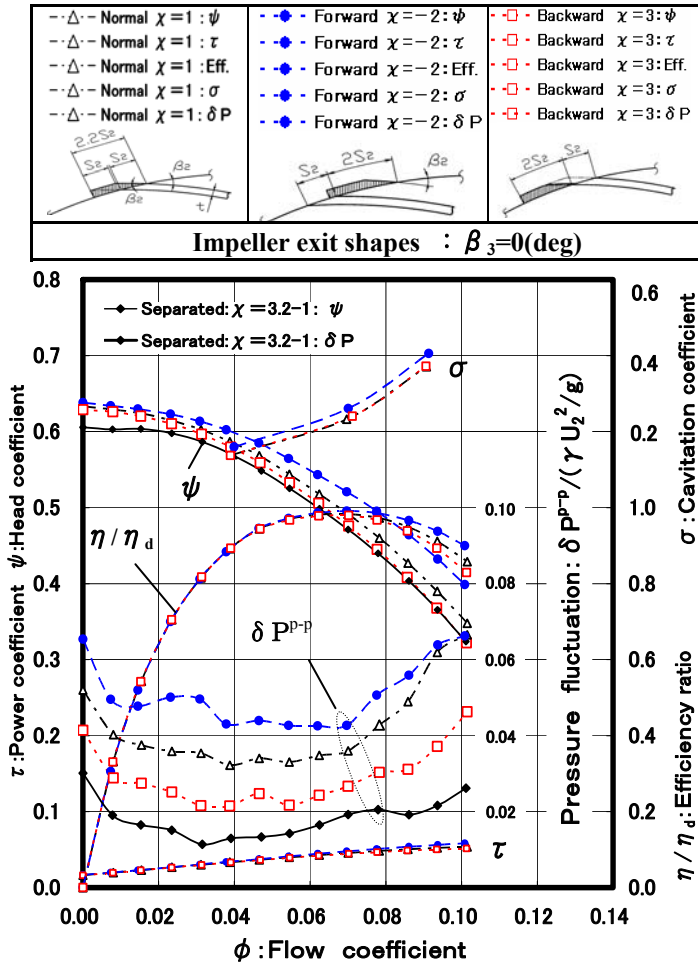
Fig. 15 Pump performance curve and δP^{p-p}
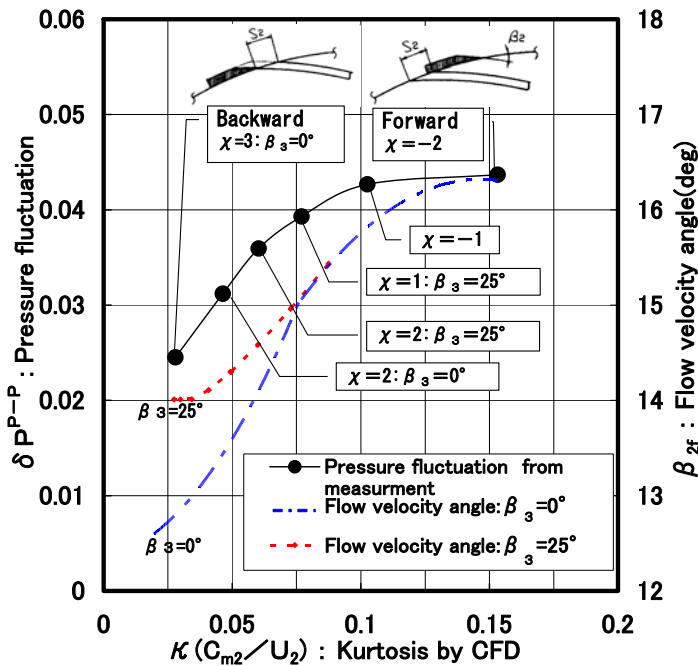(Flap exit angle: $\beta_3 = 0°$)

Fig. 16 Relation between Kurtosis and flow velocity
angle β_{2f} and pressure fluctuation ($Q/Q_d=1$)

In the case of separated cascade wing ring (Separated flap: χ=3.2-1) as shown in Fig.5(d), the pressure fluctuation and head coefficient reach the minimum. The decrement of head coefficient of the separated cascade wing ring at pump shut off point (ϕ=0) is remarkably small. Moreover, the pressure fluctuation decreases in all flowing regions. When the flap greatly moves to the suction side of impeller, it moves separately from blade trailing edge on the suction surface. It is suggested that the influence of separated flap exerts significantly on discharge flow.

When impeller vane passes the tongue of volute casing by distorting velocity distribution, the pressure fluctuation will be generated. The relationship among the pressure fluctuation δP^{p-p}, flow mean velocity angle at outlet β_{2f} and kurtosis κ is shown in Fig.16. Kurtosis κ which indicates the level of the salient of velocity distribution at impeller outlet is explained by comparing with δP^{p-p} and β_{2f}.

Kurtosis κ and β_{2f} in Fig.16 are calculated values by CFD and the pressure fluctuation is obtained from the measurement. Flow mean velocity angle at outlet β_{2f} enlarges for forward configuration (χ<0) as shown in Fig.10 and the kurtosis κ also increases.

In this case, κ grows due to the occurrence of the circumferential velocity unevenness at impeller outlet, therefore the pressure fluctuation increases as well as κ, as shown in Fig.16.

Oppositely, kurtosis κ becomes small for backward configuration (χ>1), and flow mean velocity angle at outlet β_{2f} also decreases. At this condition, the flow velocity distribution between blades at the impeller outlet becomes uniform, and the kurtosis decreases also as shown in Fig.16. The influence of blade trailing edge flap affecting on the pressure fluctuation is explained by the kurtosis κ of the flow velocity distribution at impeller outlet.

It is reported [11] that the magnitude of pressure fluctuation depends on the impeller outlet blade angle and flow rates. The pressure fluctuation has been influenced similarly by impeller outlet blade angle in this study.

The unevenness of the flow field gets larger with flow velocity angle β_{2f} at the impeller outlet. This is caused by the increment of the pressure fluctuation by the flow velocity angle β_{2f}.

Arndt, N., et al [13-14] measured the pressure fluctuations and concluded that the largest pressure fluctuations arose at the trailing edge, and that the magnitudes depended on the vane number and vane angle.

Because the kurtosis depends on the vane angle, a decrease or an increase of the pressure fluctuation could be explained by the kurtosis of the flow field at the impeller outlet, whether the impeller has a sophisticated exit shape or not.

7.3 Performance change due to attachments to blade trailing edge

Figure 17 shows the relationship between the theoretical prediction of the blade trailing edge flap extension ratio χ and the measured value of the pump head ratio. The theoretical value is obtained from eqs. (6) (7) (8).

In the backward configuration (χ>1), the pump head decreases by enlarging the blade trailing edge flap length.

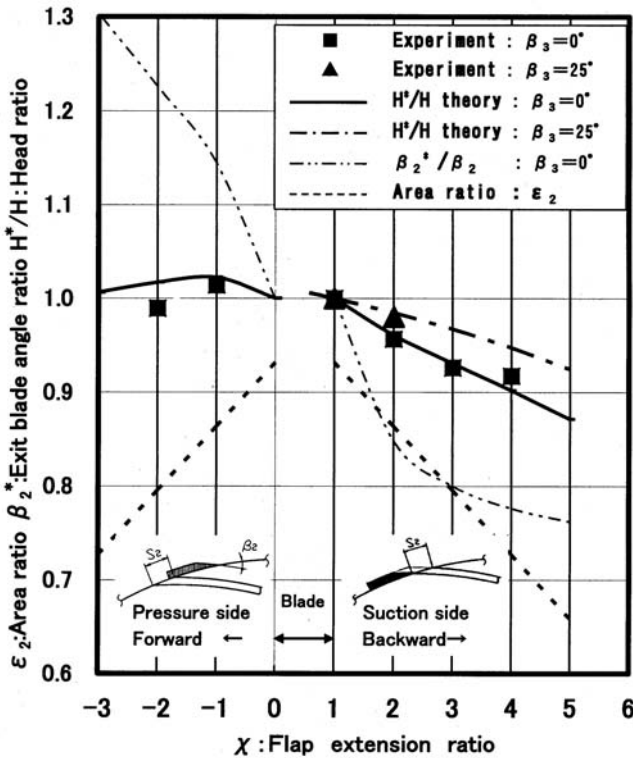**Fig. 17** Effect of flap on head prediction
comparing with experiments

The reason of the reduction can be explained that the discharge area ε_2 reduces by alternating the flow velocity angle at the impeller outlet due to trailing edge flap.

The pump head increases for the forward configuration (χ=-1). However, the pump head tends to decrease by reducing the discharge area (χ=-2) when the flap extends long enough to the direction of the pressure side.

The results of theoretical prediction show the qualitative agreement with the measured values in the range of this experiment. A little change on the pump head due to the flap position change is evaluated by eqs.(7)(8).

For the centrifugal impeller according to changing the shape of this blade trailing edge flap, the pump head and the flow rate performance can be adjusted to the specification arbitrarily.

As an example of practical use, a blade trailing edge flap is installed at the time of pump production. This blade trailing edge flap can be changed when more flowing rate and high head are needed. Therefore, the demand is easily satisfied without replacing with a large impeller [2].

7.4 Influence of blade trailing edge flap on shaft vibration

The pump flow rate ratio of Q/Q_d was fixed at 0.1, and the blade trailing edge flap is attached in the position of forward χ=-2 and backward χ=3. The pump rotational speed is changed from 600→1200→600 (min⁻¹) and then the transitional behavior of shaft vibration is analyzed by FFT as shown in Fig.18.

When the blade trailing edge flap is set to the suction side of impeller (χ=3:backward), the shaft vibration decreases. When the blade leading edge extends to the pressure side of impeller in rotational direction (χ=-2:forward) , the shaft vibration grows up the most. Because the natural frequency including the bearing support of the rotor is 113(Hz), the vane passing frequency NZ component 110(Hz) gets much more superior in case of the pump rotational speed N of 1100(min⁻¹). When blade trailing edge flap is located in pressure side of impeller as shown in Figures 14 and 15, the pressure fluctuation grows. Because the fluid excitation force depends on pressure fluctuation [12], the shaft vibration increases when the pressure fluctuation enlarges. Therefore, the small pressure fluctuation leads to the shaft vibration decreasing.
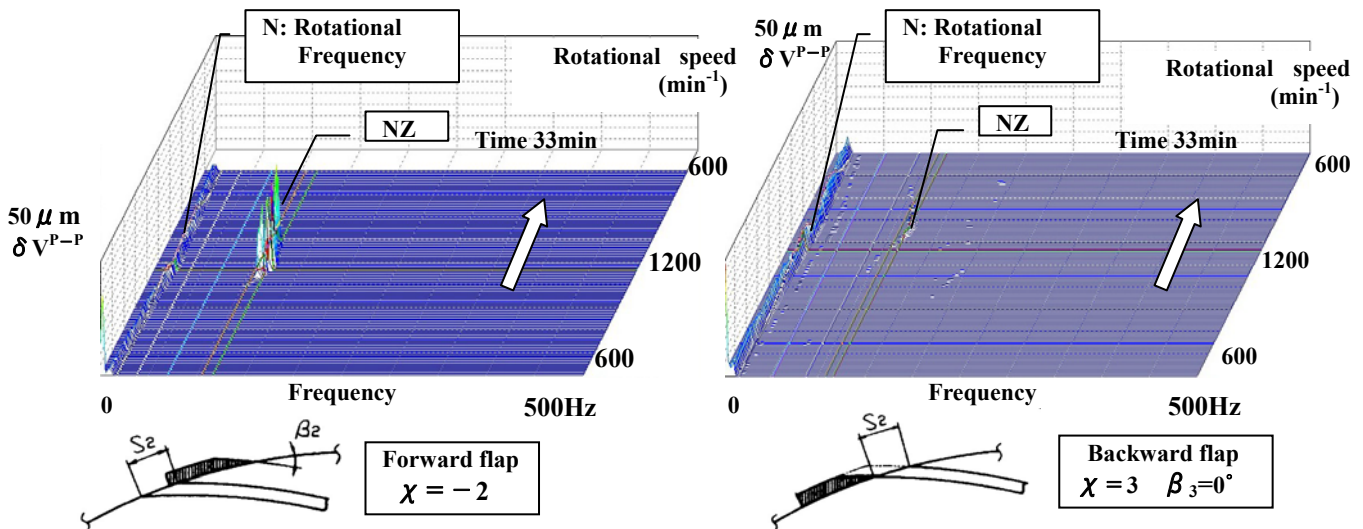

Fig. 18 FFT 3-D of rotor vibration water fall diagram $(Q/Q_d = 0.1)$

The fluid excitation force due to the pressure fluctuation increases with forward flap. Therefore, it is necessary to separate from the natural frequency enough so as not to resonate to NZ component in the pump operating speed. Moreover, when the vibration is large due to the fluid excitation force, it is reduced to low by adding the blade trailing edge flap to the suction side of impeller. As a result, it is possible to decrease the vibration by attaching a flap at impeller outlet [15].

8. Conclusions

The result of this research is summarized as follows.

An innovative method to control pump performance is proposed and performed by the formation of flaps at impeller blade outlet, instead of changing the impeller outer diameter. Without damaging either the pump efficiency or the suction performance, a technical method to adjust the pump performance is proven theoretically and experimentally by installing blade trailing edge flap in the impeller outlet of centrifugal pump. The theoretical prediction of performance change due to attachments is comparable to the experiment.

The pump shaft power and head can be reduced by attaching blade trailing edge flap to suction side of impeller blade. This is caused by a reduction in the flow velocity angle at outlet by blade trailing edge flap with the reduction of impeller discharge area. The flow velocity angle becomes smaller by extending the blade trailing edge flap in the direction of the suction side of impeller vane and kurtosis of velocity distribution between blades at impeller outlet decreases. Then the pressure fluctuation reduces as well as pump head.

On the other hand, the kurtosis grows with the flow velocity angle when blade trailing edge flap progresses in the direction of the pressure side of the impeller, and the head and the pressure fluctuation increase. It is a primary factor that the flow velocity angle at the impeller is changed by the blade trailing edge flap. The influence that the blade trailing edge flap exert on the pressure fluctuation, is explained by employing the kurtosis κ which shows the level of the salient by circumferential unevenness of the outlet flow velocity distribution.

When the blade trailing edge flap is set to the suction side of impeller (backward), the shaft vibration becomes small. Oppositely, when the blade trailing edge flap is set so as to protrude from the pressure side of impeller in rotational direction (forward), the shaft vibration grows up greatly. Therefore, the vibration can be suppressed by adding blade trailing edge flap to the suction side of impeller, when the vibration is large due to the fluid excitation force. It is suggested to decrease the vibration by attaching a flap at impeller outlet.

Nomenclature

a	The gap between tongue and casing base circle	Z	Number of vanes
B_c	Width of volute throat	β_2	Impeller blade angle at outlet
b_2	Impeller outlet discharge width	β_{2S}	Blade angle defined as （$\sin\beta_{2S}$= e /S_3）
C_{u2}	The circumference component of absolute velocity at impeller outlet	β_{2f}	Relative flow velocity angle to the direction of circumference
C_{m2}	The meridian velocity at impeller outlet	β_3	Angle of exit flap at impeller blade trailing edge
D_c	Volute base circle diameter	γ	Specific weight
D_2	Impeller outlet diameter	$\delta P^{p\text{-}p}$	Pump pressure fluctuation coefficient
e	Thickness of blade trailing edge flap		（$\delta P^{p\text{-}p} = \delta p^{p\text{-}p}/(\gamma U_2^2/g)$ ）
g	Gravitational acceleration		
k_2	Slip factor	ε_2	Impeller discharge area reduction ratio
Ns	Specific speed	η	Efficiency
	(=$NQ^{1/2}/H^{3/4}$) [min^{-1},m^3/min, m]	η_d	Efficiency at design point
n_s^*	dimensionless type number under ISO standard	κ	Kurtosis of impeller outlet velocity distribution
	{ n_s^*=2π$N Q^{1/2}/(gH)^{3/4}$ } ： 410n_s^*= Ns	ν	Angular difference ratio
S_2	Blade trailing edge length at impeller outlet	σ	Cavitation coefficient (=$2gNPSH_{req}/U_1^2$)
	(=$t/\sin\beta_2$)	τ	Power coefficient （=$L/(\rho\pi b_2 D_2 U_2^3)$）
S_3	Blade trailing edge flap length	ϕ	Flow coefficient （=$Q/\pi b_2 D_2 U_2$）
	(=$\Delta S + S_2$ or = $e/\sin\beta_{2S}$)	Ψ	Head coefficient （=$H/(U_2^2/g)$）
t	Vane thickness	χ	Blade trailing edge flap length ratio as
U_1	Peripheral velocity at the impeller eye		（= S_3 / S_2 ）
U_2	Peripheral velocity at the impeller outlet tip		When the flap progresses in the direction of the rotation, it has the sign of negative (-).
W_{u2}	The circumference component of relative velocity at impeller outlet (=U_2- C_{u2})		

Subscript ($_d$)=Pump design point   (*)=Blade trailing edge flap is applied to impeller

Abbreviation (BEP)=best efficiency point   (PS)=pressure side   (SS)=suction side

Shaft power :L and head :H per the specification of one stage impeller is used to non-dimensioning.

References

[1] Abbott.I.H. et al., 1959, "Theory of Wing Sections," p188,   Dover Publications, INC.,   McGraw–Hill.

[2] Kanemori, Y., and Pan, Y., K., 2005," Pump Performance Relative to Different Impeller Exit Blade Shapes," Turbomachinery Society of Japan, Vol. 33, No. 10, pp. 629-636. (in Japanese)

[3] Cooper, P., et al., 1994, "Computational Fluid Dynamical Analysis of Complex Internal Flows in Centrifugal Pumps," Proceedings on the 11th. International Pump Users Symposium, pp. 83-94.

[4] Majidi, K, 2005, "Numerical Study of Unsteady Flow in Centrifugal Pumps," Trans. ASME Journal of Turbo-machinery, Vol. 127, pp. 363-371.

[5] Strackeljan, J., etal. 1996, "Condition monitoring of rotating machinery using a fuzzy pattern recognition algorithm," C500/049/96,IMechE,6th.Inter. Conf. on Vib. in Rot. Machinery, pp. 507.

[6] Kurokawa, j.,, et al., 2000, " Study on Optimum Configuration of a Volute Pump of Very   Low Specific Speed," Transactions of the Japan Society of Mechanical Engineers, Series B, Vol. 66, No. 644, pp. 1132-1139. (in Japanese)

[7] Wiesner.F.J., 1967, "a Review of Slip Factors for Considering Impellers," Trans. ASME, Ser.A, 89-4, pp. 558.

[8] Ohashi, H., 1967, "Research on dynamic characteristic of turbo pump, " Transactions of the Japan Society of Mechanical Engineers, Series B, Vol. 33, No. 255, pp. 1789-1779. (in Japanese)

[9] Oono, T., et al., 1985, "Experimental Study of Pressure Fluctuation of Double Suction Centrifugal Pump," Turbomachinery Society of Japan, Vol. 13, No. 2 , pp. 21-29. (in Japanese)

[10] Maruta, Y., 1998, "Forecast and Prevention of Pump Noise," Turbomachinery Society of Japan, Vol. 26, No. 2 , pp. 42-49. (in Japanese)

[11] Iino, T., and Kasai, K.,,1985, "An Analysis of Unsteady Flow induced by Interaction Between a Centrifugal Impeller and a Vaned Diffuser, " Transactions of the Japan Society of Mechanical Engineers, Series B, Vol. 51, No. 471, pp. 3748-3753. (in Japanese)

[12] Guo, S., et al., 2005, "Measurement on the Fluid Forces Induced by Rotor-Stator Interaction in a Centrifugal Pump," Transactions of the Japan Society of Mechanical Engineers, Series B, Vol. 71, No. 706, pp. 1603-1610. (in Japanese)

[13] Arndt, N., et al., 1989, "Rotor-Stator Interaction in a Diffuser Pump," Trans.ASME Journal of Turbo-machinery, Vol. 111, pp. 213-221.

[14] Arndt, N., et al., 1990, "Experimental Investigation of Rotor-Stator Interaction in a Centrifugal Pump with Several Vaned Diffusers," Trans.ASME Journal of Turbo-machinery, Vol. 112, pp. 98-108.

[15] Kanemori, Y., 2008, JP Patent No. P4065872.